

Figure 3. Panels of identified severity grade marker candidates for HAM/TSP. Box plots of 16 peptides derived from 14 candidate proteins are displayed. The Y axis stands for the LC/MS ion intensities. *1, *2, and *3 correspond to distinct SPARC-derived peptides. Amino acid numbers of peptides are as follows: *1; 124–133, *2; 156–164, *3; 252–262. HAM/TSP, human T-cell leukemia virus-1 associated myelopathy/tropic spastic paraparesis; SPARC, secreted protein acidic and rich in cysteine.

Table 3. Clinical characteristics of the plasma specimens.

Group	N	Age (±SD)	Gender (M/F)
Training cases			
AC	37	51.5 (±13.2)	13/24
HAM1_3	4	55.0 (±4.7)	3/1
HAM4_6	20	60.5 (±10.8)	4/16
HAM7_11	10	62.0 (±8.2)	2/8
Test cases			
AC	18	54.2 (±12.3)	4/14
HAM1_3	2	59.5 (±12.0)	0/2
HAM4_6	9	56.8 (±14.9)	4/5
HAM7_11	5	71.2 (±2.9)	0/5

AC, asymptomatic carriers; HAM1_3, HAM/TSP patients whose Osame’s motor disability score range from 1 to 3; HAM4_6, HAM/TSP patients whose Osame’s motor disability score range from 4 to 6; HAM7_11, HAM/TSP patients whose Osame’s motor disability score range from 7 to 11.

ACs + HAM/TSP OMDS 1–3 with HAM/TSP OMDS 4–11 (therapeutic intervention predictor; (2)).

$$\log\left(\frac{P(x)}{1 - P(x)}\right) = -11.19 - 0.01980 (\text{SPARC}) + 0.009322 (\text{VCAM1}) + 0.1142 (\text{Viral Load}) \quad (1)$$

$$\log\left(\frac{P(x)}{1 - P(x)}\right) = -11.73 - 0.01808 (\text{SPARC}) + 0.009651 (\text{VCAM1}) + 0.09151 (\text{Viral Load}) \quad (2)$$

Finally, we assessed our prediction models using 105 plasma samples (71 training samples with 34 independent test samples). The AUC of ROC curves in Figure 4C and D demonstrated significantly higher diagnostic powers of our three-factor models for both onset prediction

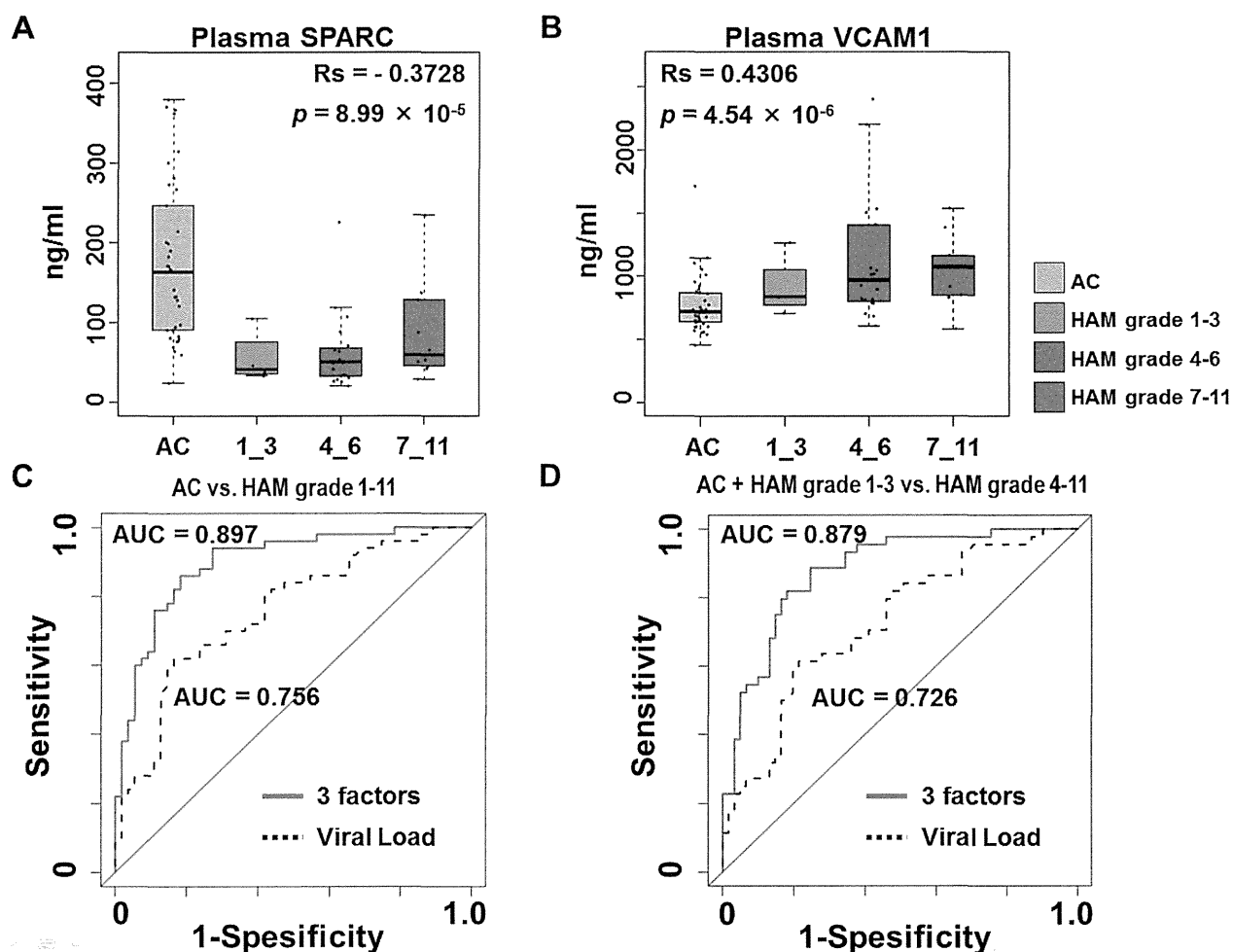


Figure 4. Construction of plasma-based diagnostic models. Plasma SPARC (A) and VCAM1 (B) were measured by ELISA assays. Pearson's correlation coefficient showed significant correlation between severity and novel markers. The three-factor logistic regression models (plasma SPARC, VCAM1, and HTLV-1 viral load) were validated with 105 samples in order for prediction of HAM/TSP onset (C) and appropriate therapeutic intervention point (D). The three-factor models showed better diagnostic performances than those of viral load only. Values of area under the curve (AUC) were shown. SPARC, secreted protein acidic and rich in cysteine; VCAM1, vascular cell adhesion molecule-1; ELISA, enzyme-linked immunosorbent assay; HTLV-1, human T-cell leukemia virus-1; HAM/TSP, human T-cell leukemia virus-1 associated myelopathy/tropic spastic paraparesis.

(AUC = 0.897) and treatment initiation point prediction (AUC = 0.879), compared to two-factor models (AUC = 0.861 and 0.856, respectively), SPARC (AUC = 0.748 and 0.736, respectively), VCAM1 (AUC = 0.768 and 0.774, respectively), and HTLV-1 viral load (AUC = 0.756 and 0.726, respectively) (Figs. S2, S3). Additionally, sensitivity and specificity of three-factor model for onset prediction were 86.0% and 81.8%, respectively, whereas those for treatment initiation point prediction were 81.8% and 82.0%, respectively (Table 4). These diagnostic yields were significantly better than those of previously reported biomarkers CSF neopterin, CSF CXCL10, and serum soluble IL-2 receptor (sIL-2R) (Table

S3). Thus, our three-factor diagnostics can provide valid and noninvasive routine test for HTLV-1 carriers and HAM/TSP patients, leading to precise disease control and better clinical outcome.

Discussion

An objective and scientifically evident diagnosis should be the basis of any medical actions. However, for HAM/TSP patients, clinical decisions have been made based on subjective health complaints mainly. Although HTLV-1 viral load, serum sIL-2R, and CSF neopterin are recently accepted as severity grade indicators for HAM/TSP,⁵ only

Table 4. Prediction of HAM/TSP onset and the point of therapeutic intervention.

Predictors	Onset					Point of therapeutic intervention				
	3 factors	SPARC + VCAM1	SPARC	VCAM1	Viral load	3 factors	SPARC + VCAM1	SPARC	VCAM1	Viral load
Training set (<i>n</i> = 71)										
Sensitivity %	85.3	82.4	76.5	79.4	55.9	80.0	73.3	76.7	60.0	53.3
Specificity %	81.1	67.6	45.9	62.2	89.2	82.9	80.5	48.8	85.4	82.9
Positive predictive value %	80.6	70.0	56.5	65.9	82.6	77.4	73.3	52.3	75.0	69.6
Negative predictive value %	85.7	80.6	68.0	76.7	68.8	85.0	80.5	74.1	74.5	70.8
AUC	0.897	0.839	0.669	0.754	0.732	0.881	0.846	0.667	0.773	0.699
Test set (<i>n</i> = 105)										
Sensitivity %	86.0	88.0	82.0	80.0	62.0	81.8	79.5	81.8	56.8	61.4
Specificity %	81.8	69.1	49.1	63.6	83.6	82.0	80.3	54.1	82.0	78.7
Positive predictive value %	81.1	72.1	59.4	66.7	77.5	76.6	74.5	56.3	69.4	67.5
Negative predictive value %	86.5	86.4	75.0	77.8	70.8	86.2	84.5	80.5	72.5	73.8
AUC	0.897	0.861	0.748	0.768	0.756	0.879	0.856	0.736	0.774	0.726

3 factors, logistic regression model using SPARC, VCAM1, and HTLV-1 viral load; HAM/TSP, human T-cell leukemia virus-1 associated myelopathy/tropic spastic paraparesis; AUC, area under the curve of ROC analysis.

relative increase/decrease of these biomarkers is valuable to assess efficiency of treatment. In this study, we successfully established predictive models which quantitatively define HAM/TSP disease status directly from plasma SPARC, VCAM1, and HTLV-1 viral load. This three-factor prediction model can be easily involved in routine medical examinations for ACs to monitor HAM/TSP onset because three biomarkers are measurable from a single blood collection without any invasive procedures such as CSF collection. Because progression of HAM/TSP tends to be rapid typically within a few years since the onset,¹² our prediction model for treatment initiation point will effectively prevent delay of deciding therapeutic intervention for early stage HAM/TSP patients.

Concerning physiological consideration of a new biomarker SPARC, the expression is specifically restricted within glial cells in nervous system including spinal cord.¹³ In addition, encephalitis induced by *N*-methyl-D-aspartic acid (NMDA) in mice resulted in downregulation of SPARC in glial cells.¹⁴ These facts suggested that plasma level of SPARC in HAM/TSP patients decrease along with the diminished number of glial cells caused by spinal cord degeneration and reduced expression of SPARC in glial cells which are pathological characteristics of HAM/TSP. On the other hand, CSF neopterin is known as an inflammatory small biological compound upregulated in many inflammatory neurologic diseases, such as multiple sclerosis, HIV encephalopathy, and Lyme neuroborreliosis,^{15–17} indicating that neopterin cannot describe spinal cord degeneration specifically. Therefore,

SPARC in plasma or CSF can be considered as more specific biomarker for HAM/TSP compared to CSF neopterin. Another new biomarker VCAM1 is expressed on the surface of endothelial cells, whose soluble form is known to be upregulated in plasma during the process of inflammation.¹⁸ In HAM/TSP patients, VCAM1 is upregulated in inflammatory region within spinal cord.¹⁹ Hence, diagnostic features of VCAM1 are more disease-oriented than neopterin, but VCAM1 can be measured from noninvasive blood specimens.

In conclusion, proteome-wide quantitative profiling of CSFs identified 14 severity grade biomarkers for HAM/TSP. Two of them, SPARC and VCAM1, were confirmed to be useful for plasma-based diagnosis of HAM/TSP onset and severity grades. It has long been difficult to expect a sudden onset of HAM/TSP after decades of asymptomatic phase in 0.5% of HTLV-1 carriers. Routine examination of our triple biomarkers will contribute to early diagnosis of HAM/TSP, leading to appropriate management of disease before suffering severe symptoms.

Acknowledgment

This work was supported by grant-in-aid for Research Project on Overcoming Intractable Diseases from the Ministry of Health Labour and Welfare Japan and grant-in-aid for Young Scientists (B) (23701090) from the Ministry of Education, Culture, Sports, Science & Technology Japan.

Conflict of Interest

Dr. Ueda has a patent Methods for detection and disease stage classification of HTLV-1 associated myelopathy pending. Dr. Ishihara has a patent Methods for detection and disease stage classification of HTLV-1 associated myelopathy pending. Dr. Araya has a patent Methods for detection and disease stage classification of HTLV-1 associated myelopathy pending. Dr. Saichi has a patent Methods for detection and disease stage classification of HTLV-1 associated myelopathy pending. Dr. Fujii has a patent Methods for detection and disease stage classification of HTLV-1 associated myelopathy pending. Dr. Sugano has a patent Methods for detection and disease stage classification of HTLV-1 associated myelopathy pending. Dr. Sato has a patent Methods for detection and disease stage classification of HTLV-1 associated myelopathy pending. Dr. Yamano has a patent Methods for detection and disease stage classification of HTLV-1 associated myelopathy pending.

References

1. Yamashita M, Ido E, Miura T, Hayami M. Molecular epidemiology of HTLV-I in the world. *J Acquir Immune Defic Syndr Hum Retrovirol* 1996;13(suppl 1):S124–S131.
2. Asquith B, Zhang Y, Mosley AJ, et al. In vivo T lymphocyte dynamics in humans and the impact of human T-lymphotropic virus 1 infection. *Proc Natl Acad Sci USA* 2007;104:8035–8040.
3. Enose-Akahata Y, Abrams A, Johnson KR, et al. Quantitative differences in HTLV-I antibody responses: classification and relative risk assessment for asymptomatic carriers and ATL and HAM/TSP patients from Jamaica. *Blood* 2012;119:2829–2836. doi: 10.1182/blood-2011-11-390807
4. Franzoi AC, Araujo AQ. Disability and determinants of gait performance in tropical spastic paraparesis/HTLV-I associated myelopathy (HAM/TSP). *Spinal Cord* 2007;45:64–68.
5. Yamano Y, Sato T. Clinical pathophysiology of human T-lymphotropic virus-type 1-associated myelopathy/tropical spastic paraparesis. *Front Microbiol* 2012;3:389. doi: 10.3389/fmicb.2012.00389
6. Kannagi M, Harashima N, Kurihara K, et al. Tumor immunity against adult T-cell leukemia. *Cancer Sci* 2005;96:249–255.
7. Shublaq M, Orsini M, Puccioni-Sohler M. Implications of HAM/TSP functional incapacity in the quality of life. *Arq Neuropsiquiatr* 2011;69(2A):208–211.
8. Semmes OJ, Cazares LH, Ward MD, et al. Discrete serum protein signatures discriminate between human retrovirus-associated hematologic and neurologic disease. *Leukemia* 2005;19:1229–1238.
9. Kirk PD, Witkover A, Courtney A, et al. Plasma proteome analysis in HTLV-1-associated myelopathy/tropical spastic paraparesis. *Retrovirology* 2011;8:81. doi: 10.1186/742-4690-8-81
10. Rahman S, Quann K, Pandya D, et al. HTLV-1 Tax mediated downregulation of miRNAs associated with chromatin remodeling factors in T cells with stably integrated viral promoter. *PLoS One* 2012;7:e34490. doi: 10.1371/journal.pone.0034490
11. Pepe MS, Cai T, Longton G. Combining predictors for classification using the area under the receiver operating characteristic curve. *Biometrics* 2006;62:221–229.
12. Taylor GP, Goon P, Furukawa Y, et al. Zidovudine plus lamivudine in human T-lymphotropic virus type-I-associated myelopathy: a randomised trial. *Retrovirology* 2006;3:63.
13. Vincent AJ, Lau PW, Roskams AJ. SPARC is expressed by macroglia and microglia in the developing and mature nervous system. *Dev Dyn* 2008;237:1449–1462.
14. Lloyd-Burton SM, York EM, Anwar MA, et al. SPARC regulates microgliosis and functional recovery following cortical ischemia. *J Neurosci* 2013;33:4468–4481.
15. Fredrikson S, Link H, Eneroth P. CSF neopterin as marker of disease activity in multiple sclerosis. *Acta Neurol Scand* 1987;75:352–355.
16. Karlens NR, Froland SS, Reinvang I. HIV-related neuropsychological impairment and immunodeficiency. CD8+ lymphocytes and neopterin are related to HIV-encephalopathy. *Scand J Psychol* 1994;35:230–239.
17. Gasse T, Murr C, Meyersbach P, et al. Neopterin production and tryptophan degradation in acute Lyme neuroborreliosis versus late Lyme encephalopathy. *Eur J Clin Chem Clin Biochem* 1994;32:685–689.
18. Devaraj S, Glaser N, Griffen S, et al. Increased monocytic activity and biomarkers of inflammation in patients with type 1 diabetes. *Diabetes* 2006;55:774–779.
19. Izumo S. Neuropathology of HTLV-1-associated myelopathy (HAM/TSP). *Neuropathology* 2010;30:480–485.

Supporting Information

Additional Supporting Information may be found in the online version of this article:

Table S1. Osame's Motor Disability Score (OMDS).

Table S2. List of peptides with the lowest 100 *P*-values.

Table S3. Prediction of HAM/TSP onset and point of therapeutic intervention with existing markers.

Figure S1. Data acquired in LC/MS/MS analyses were loaded on Refiner MS and 2D-planes represented by mass-to-charge ratio and retention time were generated. To eliminate peaks originated from chemical noises on 2D-planes, four-step Noise Subtraction was conducted. All samples were aligned by retention times and 2D-planes

were merged into a single plane to determine peptide-derived peaks in Summed Peak Detection algorithm. Quantitative information accompanying each peptide was extracted after isotope clustering and statistical analyses were performed.

Figure S2. The classifiers for HAM/TSP onset established with two factors, SPARC and VCAM1 were appraised by

area under the curve of ROC curve. Red lines indicate the ROC curves of (A) two factors, (B) SPARC, and (C) VCAM1. Black broken lines show ROC curve of viral load.

Figure S3. The classifiers which distinguished HAM 4–11 from the others were evaluated by AUC. Red lines indicate ROC curves of (A) two factors, (B) SPARC, and (C) VCAM1. Black broken lines indicate viral load.

NEW DEVELOPMENT FROM ASIA

Positive feedback loop through astrocytes causes chronic inflammation in human T-lymphotropic virus type 1-associated myelopathy/tropical spastic paraparesis

Human T-lymphotropic virus type 1 (HTLV-1) is a retrovirus infecting 10–20 million people worldwide, 2–3% of whom develop the chronic spinal cord inflammation that characterizes HTLV-1-associated myelopathy/tropical spastic paraparesis (HAM/TSP).¹ Evidence suggests that HTLV-1-infected CD4+ T cells migrate across the blood–brain barrier (BBB) and secrete pro-inflammatory cytokines, such as interferon-gamma (IFN- γ), within the central nervous system.² The present authors and others have previously shown that the chemokine CXC motif ligand 10 (CXCL10), which binds the CD4+ T helper type 1

(Th1) receptor CXC motif receptor 3 (CXCR3), stands out as particularly elevated in the cerebrospinal fluid (CSF) of HAM/TSP patients and is well-correlated with disease progression.³ We therefore hypothesized that chemokines, namely CXCL10, play an important role in the pathogenesis of HAM/TSP by continuously recruiting pro-inflammatory cells to the CNS.

We first confirmed that the CSF of HAM/TSP patients contains extraordinarily high levels of CXCL10 and CXCR3+ cells.⁴ Importantly, the levels of CXCL10 were much higher in the CSF than the

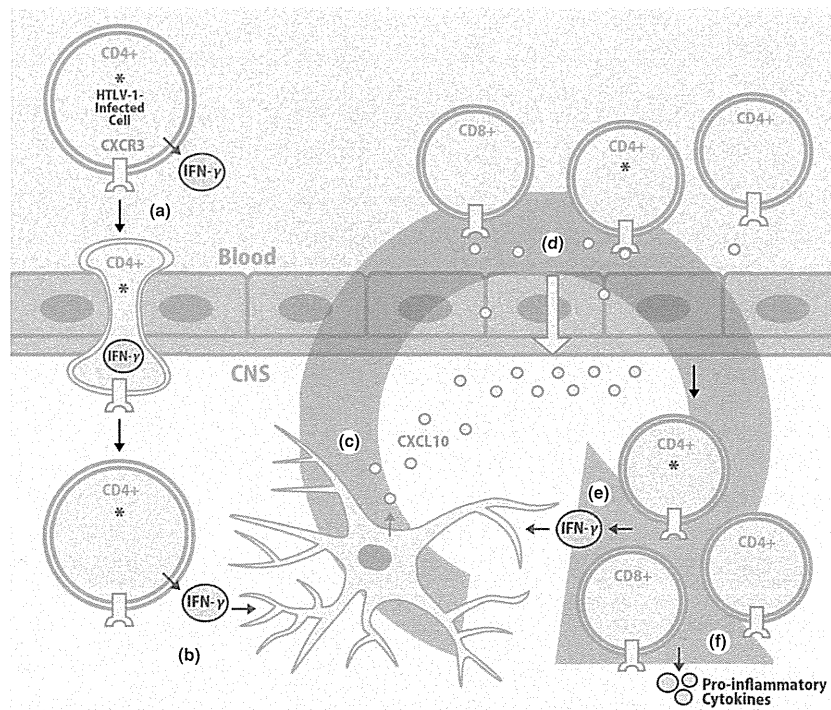


Figure 1 Human T-lymphotropic virus type 1 (HTLV-1)-associated myelopathy/tropical spastic paraparesis (HAM/TSP) pathogenesis comprises an inflammatory positive feedback loop. (a) HTLV-1-infected interferon-gamma (IFN- γ)-producing CD4+ Th1 cells migrate across the blood–brain barrier into the central nervous system, where (b) they produce IFN- γ , (c) which stimulates astrocytes to produce CXCL10. (d) The abundant CXCL10 in the central nervous system (CNS) creates a concentration gradient by which CXCR3-expressing CD4+ and CD8+ T cells undergo chemotaxis to the CNS. (e) These Th1 cells attracted by the CXCL10 also produce pro-inflammatory cytokines including IFN- γ , which further stimulates the astrocytes, (f) creating a positive feedback loop that generates abundant pro-inflammatory cytokines in the CNS. The inflammation in the CNS gradually damages the spinal cord.

serum, yielding a concentration gradient towards the CNS. Additionally, levels of CXCL10 were correlated with known features of HAM/TSP, namely increased CSF cell count. Other chemokines, such as CXCL9, CCL5 and CCL4, were considered but did not show similar trends. We then analyzed samples of peripheral blood mononuclear cells (PBMC), CSF cells, and spinal cord tissue to show that CD4+CXCR3+ cells are indeed infected with HTLV-1, do migrate across the BBB into the CNS and do produce IFN- γ in HAM/TSP patients.

Together, these results show that the pathogenesis of HAM/TSP involves CXCR3+ cells crossing the BBB, at least in part as a result of chemotactic attraction to the abundant CXCL10 in the CNS, and secreting pro-inflammatory cytokines that cause spinal cord inflammation. The question remains: from where does this abundant CXCL10 originate?

Immunohistochemical analysis of the spinal cord tissue not only confirmed that CXCL10 is produced in the spinal cords of HAM/TSP patients, but also showed that astrocytes might be the main producers. Co-culture of human astrocytoma cells with CD4+ T cells from HAM/TSP patients confirmed that astrocytes produce CXCL10 in response to IFN- γ secreted by CD4+ T cells.

We concluded that these astrocytes likely represent the missing piece of the puzzle, and we postulated the existence of an inflammatory positive feedback loop: infected CD4+ T cells cross the BBB and produce IFN- γ , which stimulates astrocytes to produce CXCL10, which recruits more CXCR3+ cells of both CD4+ and CD8+ subtypes to the CNS, where they produce more IFN- γ (Fig. 1). As for the initial trigger that starts the vicious cycle, it is thought that HTLV-1-infected cells could be inherently likely to

cross the BBB as a result of HTLV-1-induced expression of certain cell surface proteins.⁵

Finally, chemotaxis assays showed that it might be possible to disrupt this loop with anti-CXCL10 neutralizing antibodies. As the current data points to a virtually exclusively Th1-dominant pathogenesis, disruption of the Th1 inflammatory process could effectively cure the disease.

Thus, we described a Th1-centric inflammatory positive feedback loop critical for HAM/TSP pathogenesis and suggested that disrupting this loop might lead to a cure.

References

1. Osame M, Usuku K, Izumo S, et al. HTLV-I associated myelopathy, a new clinical entity. *Lancet*. 1986; **1**: 1031–2.
2. Yamano Y, Sato T. Clinical pathophysiology of human T-lymphotropic virus-type 1-associated myelopathy/tropical spastic paraparesis. *Front Microbiol*. 2012; **3**: 389.
3. Sato T, Coler-reilly A, Utsunomiya A, et al. CSF CXCL10, CXCL9, and neopterin as candidate prognostic biomarkers for HTLV-1-associated myelopathy/tropical spastic paraparesis. *PLoS Negl Trop Dis*. 2013; **7**(10): e2479.
4. Ando H, Sato T, Tomaru U, et al. Positive feedback loop via astrocytes causes chronic inflammation in virus-associated myelopathy. *Brain*. 2013; **136**(Pt 9): 2876–87.
5. Yamamoto-Taguchi N, Satou Y, Miyazato P, et al. HTLV-1 bZIP factor induces inflammation through labile Foxp3 expression. *PLoS Pathog*. 2013; **9**: e1003630.

Ariella Coler-Reilly, Hitoshi Ando and
Yoshihisa Yamano

Department of Rare Diseases Research, Institute of Medical
Science, St. Marianna University School of Medicine,
Kanagawa, Japan

CASE STUDY

Open Access

A case of post-transplant adult T-cell leukemia/lymphoma presenting myelopathy similar to but distinct from human T-cell leukemia virus type I (HTLV-I)-associated myelopathy

Toyotaka Kawamata^{1*}, Nobuhiro Ohno¹, Kota Sato^{1,2}, Masayuki Kobayashi^{1,2}, Norihide Jo¹, Koichiro Yuji¹, Ryuji Tanosaki³, Yoshihisa Yamano⁴, Arinobu Tojo^{1,2} and Kaoru Uchimaru¹

Abstract

Introduction: Adult T-cell leukemia/lymphoma (ATL) responds poorly to conventional chemotherapy, but allogeneic stem cell transplantation (allo-SCT) may improve disease prognosis. Herein, we report a female patient with human T-cell leukemia virus type I (HTLV-I)-associated myelopathy (HAM)-like myelopathy following allo-SCT for ATL.

Case report: She developed crural paresis 14 months after allo-SCT. Initially, she was diagnosed with central nervous system (CNS) relapse of ATL and treated with intrathecal injection and whole brain and spine irradiation. Her symptoms recurred 5 months later, when a cerebrospinal fluid (CSF) specimen showed increased CD4 + CXCR3 + CCR4+ cell numbers and levels of neopterin and CXCL10 (IP-10).

Discussion: These results suggest the possible involvement of a certain immunological mechanism such as HAM in her symptoms, irrespective of the lack of anti-HTLV-I antibody in her CSF. Because a definitive diagnosis of CNS manifestation of ATL is sometimes difficult, multi-modal laboratory data are required for differential diagnosis.

Keywords: Adult T-cell leukemia/lymphoma; Post-transplant myelopathy; HTLV-I-associated myelopathy (HAM); Neopterin; CXCL10 (IP-10)

Introduction

Human T-cell leukemia virus type I (HTLV-I) was the first retrovirus identified in humans, isolated from a patient with cutaneous lymphoma (Poiesz et al. 1980). HTLV-I is the cause of not only adult T-cell leukemia/lymphoma (ATL) (Uchiyama et al. 1977; Hinuma et al. 1981) but also HTLV-I-associated myelopathy (HAM)/tropical spastic paraparesis (TSP) (Osame et al. 1986), HTLV-I-associated uveitis (HU) (Ohba et al. 1989; Mochizuki et al. 1992) and infective dermatitis (McGill et al. 2012; de Oliveira et al. 2010).

ATL is one of the most intractable T-cell malignancies, and it responds poorly to conventional chemotherapy, with a median survival time (MST) of approximately

8 months (Shimoyama et al. 1988). Among such treatments, modified LSG-15 (mLSG-15) has shown the best results; in a previous study, the progression free survival (PFS) at 1 year among patients treated with mLSG-15 was 28% and the overall survival (OS) at 3 years was 24% (Tsukasaka et al. 2007). However, the improvement in survival time by mLSG-15 treatment is not satisfactory. Allo-HSCT is a promising treatment option to cure ATL because it may improve disease prognosis (Utsunomiya et al. 2001; Kami et al. 2003).

Herein, we describe a case of HAM-like myelopathy that was difficult to distinguish from central nervous system (CNS) relapse of ATL following allogeneic peripheral blood stem cell transplantation. This case report suggests that there might be immunological myelopathy after HSCT. In the present case, flow cytometric analysis of the cells in cerebrospinal fluid (CSF) was helpful to differentiate it from CNS relapse of ATL.

* Correspondence: toyotaka@ims.u-tokyo.ac.jp

¹Department of Hematology/Oncology, Research Hospital, The Institute of Medical Science, the University of Tokyo, 4-6-1 Shirokanedai, Minato-ku, Tokyo 108-8639, Japan

Full list of author information is available at the end of the article

Case report

A 63-year-old female patient recognized cervical lymph nodes swelling in October 2010. Lactate dehydrogenase (LDH) and serum corrected calcium levels kept within normal limit, but soluble interleukin-2 receptor (sIL-2R) elevated significantly at the initial visit (Table 1). Diagnostic imaging by computed tomography (CT) revealed systemic lymphadenopathies (cervical, axial, mediastinal, abdominal and mesenteric lymphadenopathy) before the following chemotherapy. Although appetite loss and abdominal distention were added with lymphadenopathy, any other abnormal finding of physical examination could not be detected. Her ECOG performance status was grade 1 before chemotherapy. She received cervical lymph node biopsy and pathological findings of cervical lymph node revealed T cell lymphoma compatible, and HTLV-I provirus DNA analysis (Southern blot) revealed monoclonal integration. Abnormal lymphocytes were not detected in peripheral blood (PB) and HTLV-I provirus DNA analysis of PB did not show monoclonal integration. She was diagnosed as ATL (lymphoma type). She has past histories of glaucoma and pulmonary cryptococcosis. None of ATL patient was in her family.

She was referred to our hospital and received four sessions of mLSG-15 therapy in our hospital. Prophylactic intrathecal injection was performed twice, during chemotherapy and before allogeneic stem cell transplantation. No meningeal involvement of ATL cells was detected at that time. She went into complete remission (Response criteria for adult T cell leukemia-lymphoma from an international consensus meeting (Tsukasaki et al. 2009)) in April 2011. She received following allogeneic peripheral blood stem cell transplantation (allo-PBSCT) in the National Cancer Center Hospital (Tokyo, Japan) (Figure 1). The transplantation conditioning regimen consisted of

fludarabine (30 mg/m² per day for 5 days) plus busulfan (3.2 mg/kg per day for 2 days) and only cyclosporine A (CyA) was used for GVHD prophylaxis. Transplanted CD34-positive cells were 2.67 × 10⁶/kg and rapid engraftment was achieved. Grade III (gastrointestinal tract and skin) acute graft-versus-host disease (GVHD) was observed 1 month after transplantation, but it improved after treatment with methylprednisolone (mPSL) (1 mg/kg). No chronic GVHD was observed. CyA was tapered gradually and discontinued 9 months after transplantation, in February 2012. After that point, only 5 mg/day prednisolone (PSL) was continued.

In July 2012 (14 months after allo-PBSCT), the patient developed hemiparesis of the left side. Although left upper-limb paresis improved, lower-extremity paresis progressed to paraplegia. Magnetic resonance imaging (MRI) revealed multiple high-intensity lesions in T2-weighted images of the medulla oblongata, cervical spinal cord, and thoracic spinal cord (Figure 2A), and a CSF specimen showed increased cell counts (Figure 3). Morphologically, typical ATL cells such as flower cells were not detected in CSF, but abnormal small to middle size lymphocytes indistinguishable from ATL cells increased. She was diagnosed as CNS relapse of ATL, and received mPSL pulse, intrathecal injection of MTX 15 mg + Ara-C 40 mg + PSL 20 mg, and irradiation of the whole brain and spine. Following these treatments, the paraplegia improved gradually to such a degree that she could walk with a walker. During the course of these treatments, she was complicated by neurogenic bladder dysfunction, and diabetes insipidus.

In January 2013 (20 months after allo-PBSCT), she again developed left lower-limb weakness, which gradually progressed. She was admitted to our hospital in February 2013. On admission, neurological examination revealed

Table 1 Laboratory data of onset of ATL (lymphoma type) in October 2010

WBC	4100/μl	GOT	67 IU/L	CRP	0.06 mg/dl
Myelo	1.0%	GPT	72 IU/L	sIL-2R	5802 U/ml
St	8.0%	LDH	215 IU/L		
Seg	71.0%	ALP	277 IU/L	HTLV-I Ab	(+)
Ly	11.0%	γ-GTP	46 IU/L	HBs-Ag	(-)
Mo	8.0%	Alb	3.5 mg/dl	HBs-Ab	(-)
Baso	1.0%	BUN	15.6 mg/dl	HBc-Ab	(-)
RBC	423 × 10 ⁴ /μl	Cre	0.58 mg/dl	HCV-Ab	(-)
Hb	13.2 g/dl	Na	142.4 mEq/L	HIV-Ab	(-)
Hct	39.0%	K	4.2 mEq/L	TPHA	(-)
MCV	92.2 fl	Cl	103.8 mEq/L		
MCH	31.2 pg	Corrected Ca	9.9 mg/dl		
MCHC	33.8%				
Plt	21.9 × 10 ⁴ /μl				

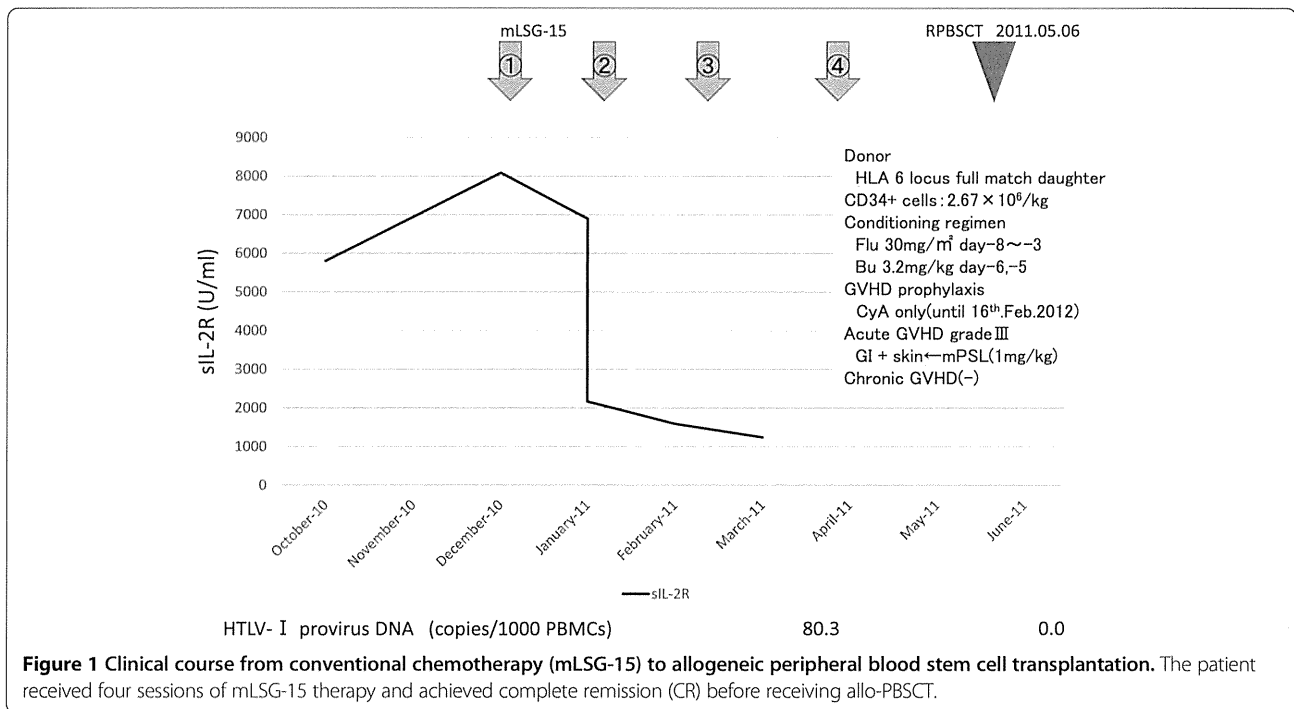


Figure 1 Clinical course from conventional chemotherapy (mLSG-15) to allogeneic peripheral blood stem cell transplantation. The patient received four sessions of mLSG-15 therapy and achieved complete remission (CR) before receiving allo-PBSCT.

no abnormality of cranial nervous system, but abnormal reflex such as Babinski and Chaddock reflex in bilateral lower-limb. Thermal hypoalgesia under right Th4 and left Th6 dermatome was detected, but tactile sense was intact. She was accompanied with bladder dysfunction and severe constipation. Brain and spinal MRI revealed a residual

spinal lesion at Th3-7 (Figure 2B). The cell numbers in CSF did not increase, but myelin basic protein (MBP) level was elevated (Figure 4B). Morphologically, ATL cells could not be detected in CSF. Flow cytometric analysis to determine the specific immunophenotype of CD4+ lymphocytes in CSF revealed an expansion of the CD4+CXCR3+CCR4+

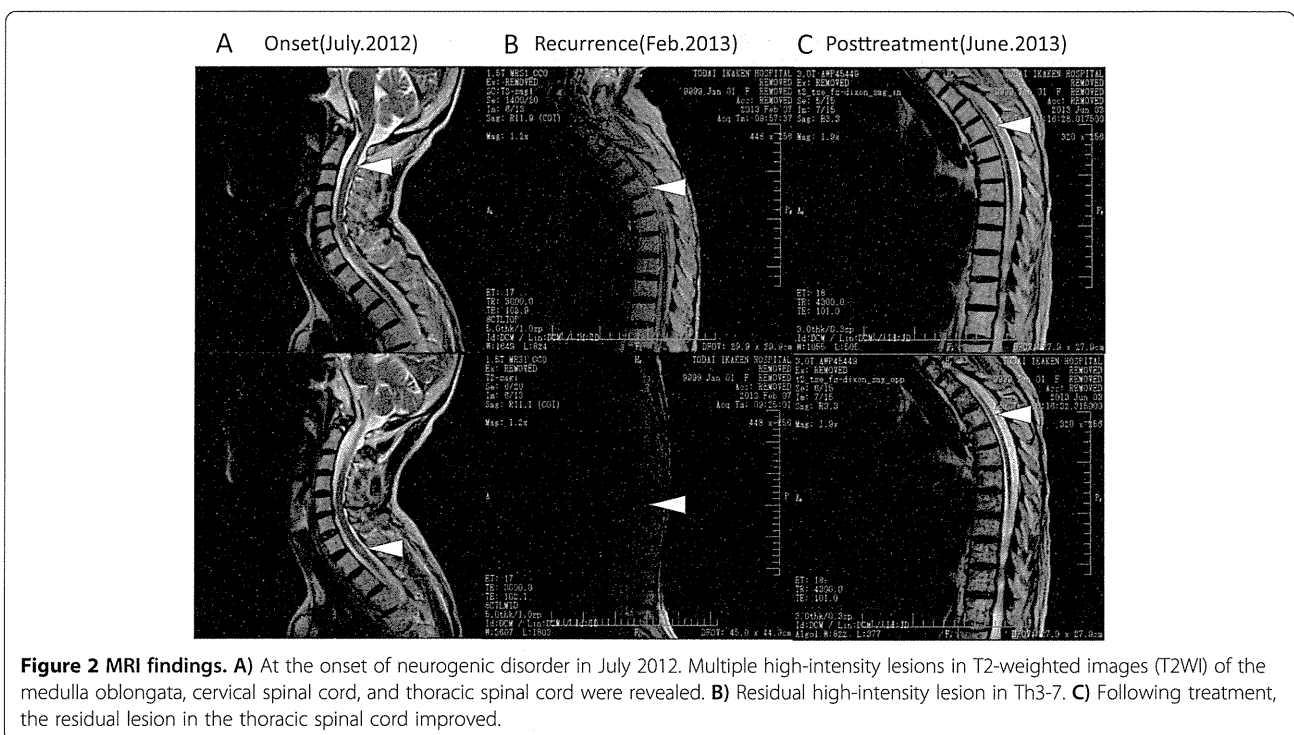


Figure 2 MRI findings. **A)** At the onset of neurogenic disorder in July 2012. Multiple high-intensity lesions in T2-weighted images (T2WI) of the medulla oblongata, cervical spinal cord, and thoracic spinal cord were revealed. **B)** Residual high-intensity lesion in Th3-7. **C)** Following treatment, the residual lesion in the thoracic spinal cord improved.

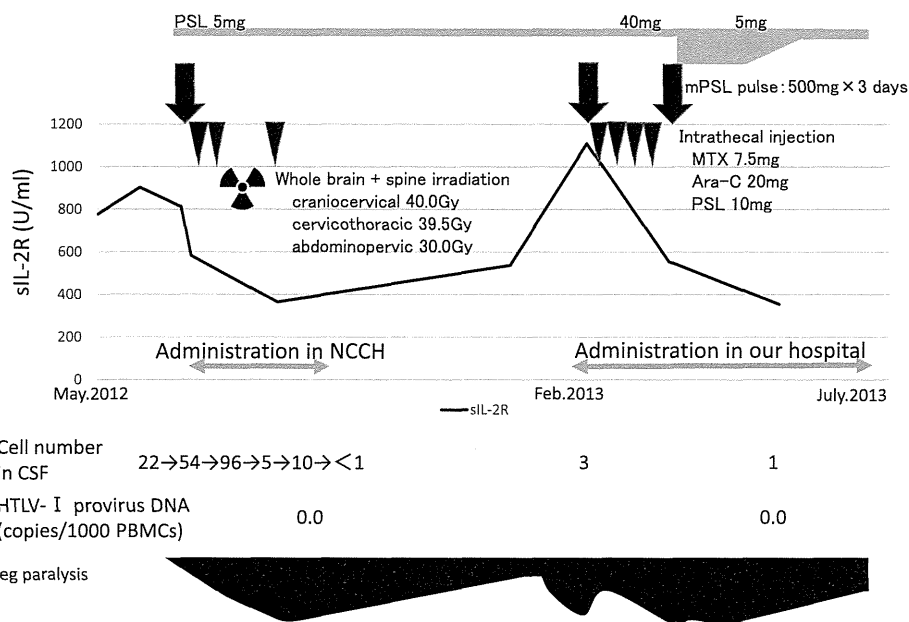


Figure 3 Clinical course after onset of the neurogenic disorder. The patient developed paraplegia 14 months after allo-PBSCT. Neurological findings were partially relieved following treatment with a high dose of mPSL accompanied by intrathecal injection of MTX + Ara-C + PSL and irradiation of the whole brain and spine. Three months later, her neurological deficit worsened again. Ultimately, her neurological disorder improved after treatment with a high dose of steroid.

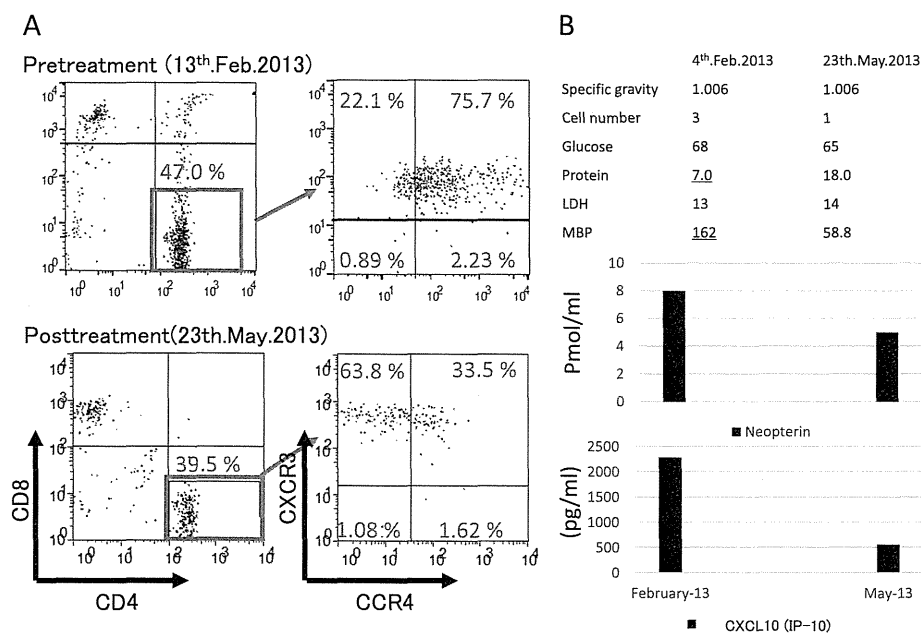


Figure 4 CSF findings. A) Flow cytometric analysis of CSF. Before treatment, the CD4 + CXCR3 + CCR4+ cell population was predominantly elevated. Following treatment, it decreased and the CD4 + CXCR3 + CCR4- cell population increased. B) Neopterin and CXCL10 (IP-10) concentrations in CSF. Before treatment, both neopterin and CXCL10 (IP-10) concentrations were significantly elevated. Following treatment, both biomarkers decreased to within the range of the therapeutic goal for HAM patients.

cell population (Figure 4A), which conflicted with CNS relapse of ATL but was consistent with HAM (Natsumi et al. 2014). Furthermore, both the neopterin and CXCL10 (IP-10) concentrations in the CSF were significantly elevated (Figure 4B), although lower than those associated with aggressive HAM (14). Notably, the case was insufficient to fulfill the diagnostic criteria for HAM (Mitsuhiro 1990) because HTLV-I antibody (PA method) was negative in CSF.

Bacterial, fungal, and tuberculous encephalomyelopathies were excluded because no increase in cell numbers and no decline in glucose concentration in CSF were observed. Real-time polymerase chain reaction (PCR) testing for CMV, EBV, HSV, VZV, HHV-6, and JC virus in CSF showed negative results.

Serum soluble interleukin-2 receptor (sIL-2R) level was slightly elevated (Table 2), but significantly lower compared with that at the onset of ATL.

Not all of the results necessarily corresponded to CNS relapse of ATL, although we could not exclude it. We treated her with mPSL pulse and intrathecal injection of MTX + Ara-C + PSL. After one course of mPSL pulse, her crural paresis improved dramatically to such a degree that she could pull up to standing after a few days. Although she was given intrathecal injections four times weekly, her crural paresis was gradually exacerbated and progressed to paralysis. mPSL pulse was performed again, but the effect was limited.

We examined her CSF again but there was no increase in cells, and ATL cells could not be detected by microscopic examination. Furthermore, the MRI findings improved over time (Figure 2C), although her neurological findings worsened and HTLV-I proviral DNA could not be detected repeatedly in peripheral mononuclear cells (PBMCs) after allo-PBSCT. No evidence of relapsed ATL could be found and we continued 5 mg/day PSL thereafter while she continued rehabilitation.

The results of CSF analysis in May 2013 showed the following improvements. In flow cytometric analysis, the CD4 + CXCR3 + CCR4+ cell population had decreased and the normal CD4 + CXCR3 + CCR4- cell population had increased. Both neopterin and CXCL10 (IP-10) had decreased to within the range of the therapeutic goal for HAM patients (Figure 4A,B). Her paralysis improved gradually and steadily only by rehabilitation, to such a degree that she could walk when holding onto parallel bars.

Discussion

ATL with CNS involvement may occur during systemic progression of the disease and its frequency is estimated to be 10–25% (Kitajima et al. 2002). However, cases of CNS relapse without peripheral blood and lymph nodes of ATL have been reported (Marshall et al. 1998; Dungenwalla et al. 2005). In flow cytometric analysis of CSF of ATL patients, the CD4 + CXCR3-CCR4+ cell population is elevated. However, in the current case, the CSF fluid analysis revealed expansion of the CD4 + CXCR3 + CCR4+ cell population, which is consistent with HAM (Natsumi et al. 2014). Sato T et al. (Sato et al. 2013) reported increased neopterin and CXCL10 (IP-10) in HAM patients, and they were valuable biomarkers for disease progression of HAM. The neopterin and CXCL10 (IP-10) concentration in CSF paralleled the disease activity of HAM. The cut-off concentrations of neopterin and CXCL10 in HAM/TSP patients compared to HTLV-I infected non-HAM subjects are less than 5 pmol/mL and 200 pg/ml, respectively, and the CXCL10 (IP-10) concentration in the CSF of HAM patients with rapid progression is usually more than 5,000 pg/mL (Yamono, Y., personal communication). In the current case, we could not make a diagnosis of HAM because the CSF was negative for HTLV-I antibody in repeated examinations. Although the immunosuppressive status after allo-PBSCT might contribute, serum immunoglobulin levels

Table 2 Laboratory data on admission to our hospital in January 2013

WBC	4470/ μ l	GOT	15 IU/L	CRP	0.24 mg/dl
St	1.5%	GPT	33 IU/L	IgG	1390 mg/dl
Seg	64.0%	LDH	199 IU/L	IgA	51 mg/dl
Ly	14.0%	ALP	453 IU/L	IgM	352 mg/dl
Mo	19.5%	γ -GTP	87 IU/L		
Abnormal Ly	1.0%	TP	6.7 mg/dl	HTLV-I Ab	(+)
RBC	$302 \times 10^4/\mu$ l	Alb	3.5 mg/dl	HBs-Ag	(-)
Hb	9.5 g/dl	BUN	9.8 mg/dl	HBs-Ab	(-)
Hct	29.4%	Cre	0.56 mg/dl	HBc-Ab	(-)
MCV	97.4 fl	Na	133 mEq/L	HCV-Ab	(-)
MCH	31.5 pg	K	4.0 mEq/L	HIV-Ab	(-)
MCHC	32.3%	Cl	96 mEq/L		
Plt	$12.0 \times 10^4/\mu$ l	Corrected Ca	10.5 mg/dl		

were almost within normal limit at the same time period (Table 2) and there is not enough evidence to indicate false negative. In any inflammatory diseases of CNS, CXCR3+ cells but not CCR4+ cells were generally found in CSF (Misu et al. 2001). However, CXCR3 + CCR4+ double positive cells existed in her CSF. It was unlikely that CXCR3 + CCR4+ double positive cells emerged into CSF in nonspecific inflammatory condition. Given her background, we supposed these CCR4+ cells were HTLV-I infected cells, but the number of these cells was insufficient to measure HTLV-I viral load.

In the current case, neither CSF data nor clinical course consisted with CNS relapse of ATL. In case of ATL patients, CXCR3-CCR4+ T cell lymphocytes population expanded. Therapeutic effect was obtained from mPSL pulse rather than intrathecal injection. Furthermore, disease progression in the typical case of CNS relapse of ATL was more aggressive. We concluded some inflammatory condition caused by these HTLV-I infected cells may have developed HAM-like myelopathy.

CNS GVHD remains a controversial entity and it is difficult to establish an unequivocal diagnosis. Yet a few cases have been reported, who were suspected of CNS GVHD from brain biopsy or autopsy, their CSF showed predominant T-lymphocyte infiltration of donor origin (Kamble et al. 2007). In the current case, brain or spinal cord biopsy was not performed, and chimerism analysis of T cells in CSF was difficult because of the full-match HLA and sex-matched PBSCT. The number of T cells in CSF was insufficient to analyze chimerism using the short tandem repeat (STR) method. Neopterin (Niederwieser et al. 1984; Hempel et al. 1997) and CXCL10 (IP-10) (Mapara et al. 2006) levels in serum increase significantly in patients with active GVHD, but the levels in CSF are unknown. The possibility of active CNS GVHD could not be completely excluded. Both CXCR3 and CCR4 expression of T cells infiltrated in the CNS in patients with active CNS GVHD is unknown. It was no wonder that CXCR3+ cells in CSF were found in nonspecific inflammatory condition such as CNS GVHD, but unlikely that CCR4+ cells were.

The patient's neurological dysfunction seemed to fluctuate in parallel with the serum concentration of soluble interleukin-2 (sIL-2R) receptor (Figure 3). However, increased sIL-2R occurs not only with ATL relapse but also with HAM (Matsumoto et al. 1990), GVHD (Kami et al. 2000), and inflammatory neurogenic disorders caused by immunologic T-cell responses (Maier et al. 2009). Thus, it is difficult to make a definite diagnosis based on elevated sIL-2R alone.

In conclusion, we report a case with myelopathy without ATL relapse in the CNS. Flow cytometric analysis is helpful to differentiate immune-mediated encephalopathy or myelopathy from CNS relapse of ATL. If we encountered the patients suspected of CNS relapse of ATL, we should

consider the possibility of inflammatory condition caused by HTLV-I infected cells. Further analysis of pathology are warranted.

Competing interests

The authors declare that they have no competing interests.

Authors' contribution

TK participated in treatment for the patient and drafting the manuscript. NO, KS, MK, NJ and KY participated in treatment for the patient. YY carried out flow cytometric analysis and measurement of neopterin and CXCL10 (IP-10) concentration in CSF, and helped to draft the manuscript. RT participated in acquiring the data and helping to draft the manuscript. AT and KU supervised and helped to draft the manuscript. All authors read and approved the final manuscript.

Author details

¹Department of Hematology/Oncology, Research Hospital, The Institute of Medical Science, the University of Tokyo, 4-6-1 Shirokanedai, Minato-ku, Tokyo 108-8639, Japan. ²Division of Molecular Therapy, Department of The advanced Clinical Research Center, The Institute of Medical Science, the University of Tokyo, 4-6-1 Shirokanedai, Minato-ku, Tokyo 108-8639, Japan. ³Department of Blood Transfusion and Cellular Therapy, National Cancer Center Hospital, 5-1-1 Tsukiji, Chuo-ku, Tokyo 104-0045, Japan. ⁴Department of Rare Diseases Research, Institute of Medical Science, St. Marianna University Graduate School of Medicine, Sugao, Miyamae-ku, Kawasaki, Kanagawa 216-8512, Japan.

Received: 15 August 2014 Accepted: 22 September 2014

Published: 4 October 2014

References

- de Oliveira MF, Vieira M, Primo J, Siqueira IC, Carvalho EM, Farre L, Fatal PL, Bittencourt AL (2010) Flower cells in patients with infective dermatitis associated with HTLV-1. *J Clin Virol* 48:288–290
- Dungerwalla M, Osuji N, Waldman AD, Jehani FAI, Mehta A, Taylor R, Wotherspoon A, Cogill G, Matutes E (2005) Isolated central nervous system involvement in adult T-cell lymphoma/leukaemia. *Br J Haematol* 130:511–515
- Hempel L, Köhrholz D, Nussbaum P, Bönig H, Burdach S, Zintl F (1997) High interleukin-10 serum levels are associated with fatal outcome in patients after bone marrow transplantation. *Bone Marrow Transplant* 20:365–368
- Hinuma Y, Nagata K, Hanaoka M, Nakai M, Matsumoto T, Kinoshita K, Shirakawa S, Miyoshi I (1981) Adult T-cell leukemia: antigen in an ATL cell line and detection of antibodies to the antigen in human sera. *Proc Natl Acad Sci U S A* 78:6476–6480
- Kamble RT, Chang CC, Sanchez S, Carrum G (2007) Central nervous system graft-versus-host disease: report of two cases and literature review. *Bone Marrow Transplant* 39:49–52
- Kami M, Matsumura T, Tanaka Y, Mikami Y, Miyakoshi S, Ueyama J, Morinaga S, Mori S, Machida U, Kanda Y, Chiba S, Sakamaki H, Hirai H, Muto Y (2000) Serum levels of soluble interleukin-2 receptor after bone marrow transplantation: a true marker of acute graft-versus-host disease. *Leuk Lymphoma* 38:533–540
- Kami M, Hamaki T, Miyakoshi S, Murashige N, Kanda Y, Tanosaki R, Takaue Y, Taniguchi S, Hirai H, Ozawa K, Kasai M (2003) Allogeneic haematopoietic stem cell transplantation for the treatment of adult T-cell leukaemia/lymphoma. *Br J Haematol* 120:304–309
- Kitajima M, Korogi Y, Shigematsu Y, Murashige M, Kanda Y, Tanosaki R, Takaue Y, Taniguchi S, Hirai H, Ozawa K, Kasai M (2002) Central nervous system lesions in adult T-cell leukaemia: MRI and pathology. *Neuroradiology* 44:559–567
- Maier LM, Anderson DE, Severson CA, Baecher-Allan C, Healy B, Liu DV, Wittrup KD, De Jager PL, Hafler D (2009) Soluble IL-2RA levels in multiple sclerosis subjects and the effect of soluble IL-2RA on immune responses. *J Immunol* 182:1541–1547
- Mapara MY, Leng C, Kim YM, Bronson R, Loksbin A, Luster A, Sykes M (2006) Expression of chemokines in GVHD target organs is influenced by conditioning and genetic factors and amplified by GVHR. *Biol Blood Marrow Transplant* 12:623–634
- Marshall AG, Pawson R, Thom M, Shuz TF, Scaravilli F, Rudge P (1998) HTLV-I associated primary CNS T-cell lymphoma. *J Neurol Sci* 158:226–231
- Matsumoto M, Sugimoto M, Nakashima H, Imamura F, Kawano O, Uyama E, Takatsu K, Araki S (1990) Spontaneous T cell proliferation and release of

- soluble interleukin-2 receptors in patients with HTLV-I-associated myelopathy. *Am J Trop Med Hyg* 42:365–373
- McGill NK, Vyas J, Shimauchi T, Tokura Y, Piguet V (2012) HTLV-1-associated infective dermatitis: updates on the pathogenesis. *Exp Dermatol* 21:815–821
- Misu T, Onodera H, Fujihara K, Matsushima K, Yoshie O, Okita N, Takase S, Itoyama Y (2001) Chemokine receptor expression on T cells in blood and cerebrospinal fluid at relapse and remission of multiple sclerosis: imbalance of Th1/Th2-associated chemokine signaling. *J Neuroimmunol* 114:207–212
- Mitsuhiro O (1990) Review of WHO kagoshima meeting and diagnostic guidelines for HAM/TSP. Raven Press, New York, pp 191–197
- Mochizuki M, Watanabe T, Yamaguchi K, Yoshimura K, Nakashima S, Shirao M, Araki S, Takatsuki K, Mori S, Miyata N (1992) Uveitis associated with human T-cell lymphotropic virus type I. *Am J Ophthalmol* 114:123–129
- Natsumi A, Tomoo S, Hitoshi A, Yoshihisa Y (2014) HTLV-1 induces a Th1-like state in CD4+CCR4+ T cells. *J Clin Invest* 124:3431–3442
- Niederwieser D, Huber C, Gratwohl A, Bannert P, Fuchs D, Hausen A, Reibnegger D, Speck B, Wachter H (1984) Neopterin as a new biochemical marker in the clinical monitoring of bone marrow transplant recipients. *Transplantation* 38:497–500
- Ohba N, Matsumoto M, Sameshima M, Kabayama Y, Nakao K, Unoki K, Uehara F, Kawano K, Maruyama I, Osame M (1989) Ocular manifestations in patients infected with human T-lymphotropic virus type I. *Jpn J Ophthalmol* 33:1–12
- Osame M, Usuku K, Izumo S, Ijichi N, Amitani H, Igata A, Matsumoto M, Tara M (1986) HTLV-I associated myelopathy, a new clinical entity. *Lancet* 1:1031–1032
- Poiesz BJ, Ruscetti FW, Gazdar AF, Bunn PA, Minna JD, Gallo RC (1980) Detection and isolation of type C retrovirus particles from fresh and cultured lymphocytes of a patient with cutaneous T-cell lymphoma. *Proc Natl Acad Sci U S A* 77:7415–7419
- Sato T, Coler-Reilly A, Utsunomiya A, Araya N, Yagishita N, Ando H, Yamauchi J, Inoue E, Ueno T, Hasegawa Y, Nishioka K, Nagajima T, Jacobson S, Izumo S, Yamano Y (2013) CSF CXCL10, CXCL9, and neopterin as candidate prognostic biomarkers for HTLV-1-associated myelopathy/tropical spastic paraparesis. *PLoS Negl Trop Dis* 7:e2479
- Shimoyama M, Ota K, Kikuchi M, Yunoki K, Konda S, Takatsuki K, Ichimaru M, Tominaga S, Tsugane S, Minato K, Tobinai K, Oyama A, Hisano S, Matsumoto M, Takiguchi T, Yamaguchi K, Kinoshita K, Tajima K, Suemasu K (1988) Major prognostic factors of adult patients with advanced T-cell lymphoma/leukemia. *J Clin Oncol* 6:1088–1097
- Tsukasaki K, Utsunomiya A, Fukuda H, Shibata T, Fukushima T, Takatsuka Y, Ikeda S, Masuda M, Nagoshi H, Ueda R, Tamura K, Sano M, Momita S, Yamaguchi K, Kawano F, Hanada S, Tobinai K, Shimoyama M, Hotta T, Tomonaga M (2007) VCAP-AMP-VECP compared with biweekly CHOP for adult T-cell leukemia-lymphoma: Japan Clinical Oncology Group Study JCOG9801. *J Clin Oncol* 25:5458–5464
- Tsukasaki K, Hermine O, Bazarbachi A, Ratner L, Ramos JC, Harrington W, Jr, O'Mahony D, Janik JE, Bittencourt AL, Taylor GP, Yamaguchi K, Utsunomiya A, Tobinai K, Watanabe T (2009) Definition, prognostic factors, treatment, and response criteria of adult T-cell leukemia-lymphoma: a proposal from an international consensus meeting. *J Clin Oncol* 27:453–459
- Uchiyama T, Yodoi J, Sagawa K, Takatsuki K, Uchino H (1977) Adult T-cell leukemia: clinical and hematologic features of 16 cases. *Blood* 50:481–492
- Utsunomiya A, Miyazaki Y, Takatsuka Y, Hanada S, Uozumi K, Yashiki S, Tara M, Kawano F, Saburi Y, Kikuchi H, Hara M, Sao H, Morishima Y, Kodaera Y, Sonoda S, Tomonaga M (2001) Improved outcome of adult T cell leukemia/lymphoma with allogeneic hematopoietic stem cell transplantation. *Bone Marrow Transplant* 27:15–20

doi:10.1186/2193-1801-3-581

Cite this article as: Kawamata *et al.*: A case of post-transplant adult T-cell leukemia/lymphoma presenting myelopathy similar to but distinct from human T-cell leukemia virus type I (HTLV- I)-associated myelopathy. *SpringerPlus* 2014 **3**:581.

Submit your manuscript to a SpringerOpen® journal and benefit from:

- Convenient online submission
- Rigorous peer review
- Immediate publication on acceptance
- Open access: articles freely available online
- High visibility within the field
- Retaining the copyright to your article

Submit your next manuscript at ► springeropen.com

Regular Article

LYMPHOID NEOPLASIA

An animal model of adult T-cell leukemia: humanized mice with HTLV-1-specific immunity

Kenta Tezuka, Runze Xun, Mami Tei, Takaharu Ueno, Masakazu Tanaka, Norihiro Takenouchi, and Jun-ichi Fujisawa

Department of Microbiology, Kansai Medical University, Hirakata, Osaka, Japan

Key Points

- Humanized mice, IBMI-huNOG, were generated by intra-bone marrow injection of human CD133⁺ hematopoietic stem cells.
- HTLV-1-infected IBMI-huNOG mice recapitulated distinct ATL-like symptoms as well as HTLV-1-specific adaptive immune responses.

Human T-cell leukemia virus type 1 (HTLV-1) is causally associated with adult T-cell leukemia (ATL), an aggressive T-cell malignancy with a poor prognosis. To elucidate ATL pathogenesis *in vivo*, a variety of animal models have been established; however, the mechanisms driving this disorder remain poorly understood due to deficiencies in each of these animal models. Here, we report a novel HTLV-1-infected humanized mouse model generated by intra-bone marrow injection of human CD133⁺ stem cells into NOD/Shi-scid/IL-2R γ c null (NOG) mice (IBMI-huNOG mice). Upon infection, the number of CD4⁺ human T cells in the periphery increased rapidly, and atypical lymphocytes with lobulated nuclei resembling ATL-specific flower cells were observed 4 to 5 months after infection. Proliferation was seen in both CD25⁻ and CD25⁺ CD4 T cells with identical proviral integration sites; however, a limited number of CD25⁺-infected T-cell clones eventually dominated, indicating an association between clonal selection of infected T cells and expression of CD25. Additionally, HTLV-1-specific adaptive immune responses were induced in infected mice and

might be involved in the control of HTLV-1-infected cells. Thus, the HTLV-1-infected IBMI-huNOG mouse model successfully recapitulated the development of ATL and may serve as an important tool for investigating *in vivo* mechanisms of ATL leukemogenesis and evaluating anti-ATL drug and vaccine candidates. (*Blood*. 2014;123(3):346-355)

Introduction

Human T-cell leukemia virus type 1 (HTLV-1) is a retrovirus associated with adult T-cell leukemia (ATL) and HTLV-1-associated myelopathy or tropical spastic paraparesis (HAM/TSP) in humans.¹⁻³ Although the majority of HTLV-1-infected individuals remain asymptomatic throughout their lives, approximately 5% of HTLV-1 carriers develop ATL or HAM/TSP following a long latency period.⁴ In addition to the classic structural proteins required for retroviral replication, the HTLV-1 proviral genome encodes several accessory and regulatory proteins, including the viral transcriptional activator Tax and the HTLV-1 bZIP factor (HBZ), which are thought to be linked to HTLV-1 pathogenesis.^{5,6}

ATL is an aggressive malignancy of mature CD4 T cells, characterized by frequent visceral involvement, lymphadenopathy, hypercalcemia or hypercytokinemia, and monoclonal proliferation of HTLV-1-infected tumor cells.⁷ Typical ATL cells exhibit an unusual morphology with lobulated nuclei, known as “flower cells.”⁸ These cells are also characterized by their robust expression of interleukin (IL)-2 receptor α (CD25).⁹

To reproduce the pathogenesis of ATL, a number of mouse models have been developed, including transgenic or xenografted/humanized mice.¹⁰⁻¹⁸ One such model is the Tax-transgenic mouse, which expresses Tax under the control of the Lck promoter. This

model restricts Tax expression to developing thymocytes, resulting in characteristic ATL-like phenotypes.¹⁵ Another model, the HBZ-transgenic mouse, expresses HBZ under the control of a CD4-specific promoter/enhancer/silencer. These mice develop lymphomas characterized by induction of Foxp3 in CD4 T cells, similar to leukemic cells in ATL patients.¹⁸ These observations clearly demonstrate that the leukemogenic activity of not only Tax but also HBZ is related to the development of ATL.

In addition to transgenic mouse models, a variety of HTLV-1-infected small-animal models have been established to evaluate viral pathogenesis and elucidate the function of viral products *in vivo*.^{19,20} These infection models have provided valuable findings regarding virus-host interactions; however, they are unable to fully recapitulate pathological conditions resembling ATL, likely due to the low efficiency of HTLV-1 infection.

Humanized mice are highly susceptible to infection with human lymphotropic viruses such as EBV, HIV-1, and HTLV-1, and have been used to recapitulate specific disorders and human immune responses.^{17,21,22} Recent studies on HTLV-1 infection in humanized mouse models successfully reproduced HTLV-1-associated T-cell lymphomas^{16,17}; however, these models did not accurately recreate human immune responses against HTLV-1.

Submitted June 17, 2013; accepted October 27, 2013. Prepublished online as *Blood* First Edition paper, November 6, 2013; DOI 10.1182/blood-2013-06-508861.

The online version of this article contains a data supplement.

There is an Inside *Blood* commentary on this article in this issue.

The publication costs of this article were defrayed in part by page charge payment. Therefore, and solely to indicate this fact, this article is hereby marked “advertisement” in accordance with 18 USC section 1734.

© 2014 by The American Society of Hematology

Notably, humoral immunity, along with cytotoxic T cell (CTL)-mediated cytotoxicity, is thought to play a pivotal role in controlling the proliferation or selection of HTLV-1–infected T-cell clones *in vivo*.^{23,24} It is therefore important to develop mouse models of ATL that induce more human-like HTLV-1–specific immune responses.

In this study, we describe a novel humanized mouse model of HTLV-1 infection in the presence of specific adaptive immune responses. Our novel HTLV-1–infected humanized mice displayed distinct ATL-like symptoms, including hepatosplenomegaly, hypercytokinemia, oligoclonal proliferation of HTLV-1–infected T cells, and the appearance of flower cells. In addition, HTLV-1–specific immunity was induced and may be involved in the control of infected cells *in vivo*.

Materials and methods

Purification of human CD133⁺ cells from cord blood

Cord blood samples from full-term human deliveries were obtained from the Japanese Red Cross Kinki Cord Blood Bank (Osaka, Japan) for research use due to the inadequate numbers of stem cells for human transplantation; all patients provided signed, informed consent in accordance with the Declaration of Helsinki. Mononuclear cells (MNCs) were separated using Ficoll-Conray (Lymphosepar I, IBL) density gradient centrifugation. After collecting MNCs, a CD133 MicroBead Kit (Miltenyi Biotec) was used to isolate human CD133⁺ cells (Miltenyi Biotec) according to the manufacturer's instructions. HLA-A typing was performed using a WAKFlow HLA typing kit (WAKUNAGA) according to the manufacturer's instructions; the results are shown in supplemental Table 1 (available on the *Blood* Web site).

NOG mice

Female 6-week-old NOD/Shi-scld/IL-2R γ c null (NOG) mice²⁵ were purchased from the Central Institute of Experimental Animals (Kawasaki, Japan). Mice were handled under sterile conditions and were maintained in germ-free isolators. All animal experiments were approved by the Animal Care Committees of Kansai Medical University.

Generation of IBMI-huNOG

Seven-week-old NOG mice were sublethally irradiated with 250 cGy from a ¹³⁷Cs source (Gammacell 40 exactor, Nordion International). Within 24 hours of irradiation, each mouse was injected with 5×10^4 human CD133⁺ cells by intra-bone marrow injection (IBMI)²⁶ as reported previously.²⁷

HTLV-1 infection to IBMI-huNOG

The HTLV-1–infected T-cell line MT2²⁸ was irradiated with 10 Gy from a ¹³⁷Cs source irradiator. Irradiated MT2 cells (2.5×10^6) or phosphate-buffered saline were inoculated intraperitoneally into 24- to 28-week-old IBMI-huNOG mice. Mice were anesthetized and killed when the body weight decreased to <70% of their maximum weight. Peripheral blood smears were prepared using May-Grunwald Giemsa staining and examined by light microscopy. All infections were performed in a Biosafety Level P2A laboratory in accordance with the guidelines of Kansai Medical University.

Flow cytometric analysis and cell sorting

Peripheral blood cells were routinely collected every 2 weeks after infection, and after sacrificing mice, single-cell suspensions of various lymphoid tissues were prepared as described previously.²⁹ To stain surface markers, anti-human CD45-PerCP or APC-Cy7, CD3–fluorescein isothiocyanate (FITC) or phycoerythrin (PE)-Cy7, CD4-PE, CD8-PerCP-Cy5.5, CD19-PE, CD25-FITC, CCR4-APC antibodies were used, along

with mouse immunoglobulin G1 and FITC as an isotype control (all BD Biosciences). AccuCount Ultra Rainbow Fluorescent Particles (Spherotech) were employed to determine absolute cell numbers, according to the manufacturer's protocol. Flow cytometric analysis was performed on a BD FACScan for 3-color staining and a BD FACScan II (BD Biosciences) for 7-color staining. The CellQuest and Diva software programs were used for data acquisition (BD Biosciences), and the collected data were analyzed by FCS express 3 (De Novo Software). Human CD4+, CD8-, and CD25-expressing T cells were sorted from splenic MNCs by FACSARIA or FACSARIA III (BD Biosciences).

Tetramer staining

PE-conjugated HLA-A*24:02/Tax301-309 (SFHSLHLLF) and HLA-A*24:02/HIV (RYLRDQQL) env gp160 tetramers were purchased from MBL. Splenocytes from mock-infected or HTLV-1–infected mice were stained with each tetramer and anti-human CD3 and CD8 antibodies according to the manufacturer's protocol. Mixed lymphocyte-peptide cultures were performed to stimulate Tax-specific CTLs, as described previously.³⁰ Briefly, splenocytes from HTLV-1–infected mice were cultured for 13 days with 10 mg/mL Tax301-309 peptide and 50 U/mL recombinant human IL-2 (Takeda Chemical Industries). Cultured splenocytes were then analyzed by flow cytometry.

DNA isolation and quantification of proviral load

Genomic DNA was extracted from single-cell suspensions of tissue or peripheral blood using a conventional phenol extraction method. Proviral loads (PVLs) were measured by quantitative polymerase chain reaction (PCR) using a MyiQ or CFX96 real-time PCR system (Bio-Rad). The primers and probes targeting for HTLV-1 *pX* and human β -globin (HBB; as an internal control) are listed in supplemental Table 2. A plasmid containing PCR fragments for the HTLV-1 *pX* region and HBB was constructed using T-Vector pMD20 (TaKaRa) and used as the quantified standard template for real-time PCR.³¹ The PVL was calculated as: [(copy number of *pX*)/(copy number of HBB / 2)] \times 100.

Quantification of clonal occupancy by clone-specific PCR

Inverse long PCR (IL-PCR) was performed to amplify the genomic DNA flanked the 3' long terminal repeat of HTLV-1 provirus according to a modified method described previously.³² In brief, the genomic DNA was digested by *Pst*I, self-ligated by T4 ligase, and then digested by *Mlu*I. Long PCR amplification of the linearized DNA was performed using the PrimeSTAR GXL DNA polymerase (TaKaRa) according to the manufacturer's protocol. Primer sets for IL-PCR analysis are listed in supplemental Table 3. IL-PCR products were isolated from agarose gels, purified, and subjected to nested PCR. Amplified nested PCR fragments were subcloned into T-Vector pMD20 (TaKaRa) and sequenced to obtain provirus integration sites downstream of the 3' long terminal repeat. Integration site-specific primers were designed based on the DNA sequence of the flanking region of the provirus derived from splenic DNA of 8 HTLV-1–infected mice, and are listed in supplemental Table 5. A detailed description of the clone-specific quantitative PCR procedure has been provided elsewhere.³³ The clonal occupancy of each clone was calculated as: [(copy number of integration sites)/(copy number of *pX*)] \times 100.

Real-time RT-PCR to quantify *tax* and *HBZ* transcripts

Total RNA was isolated using the TRIzol reagent (Invitrogen) and complementary DNA samples were synthesized from 1 μ g total RNA. Reverse-transcription PCR (RT-PCR) was performed by the use of SsoFast EvaGreen Supermix (Bio-Rad). Primers used for RT-PCR are listed in supplemental Table 4. Relative expression levels were calculated by the MyiQ system (Bio-Rad).

Titration of HTLV-1–specific antibodies

The titers of antibodies against HTLV-1 antigens in the plasma of infected mice were determined by the particle agglutination method using Serodia

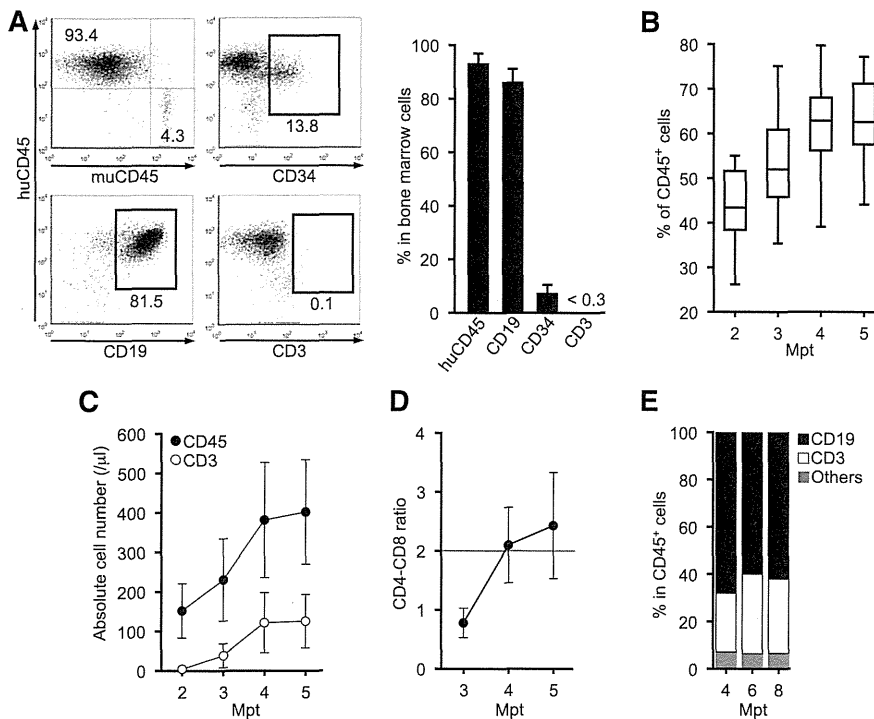


Figure 1. Generation of IBMI-huNOG mice and T-cell development in periphery. (A) Development of human leukocytes in bone marrow of IBMI-huNOG mice. Bone marrow cells from IBMI-huNOG mice ($n = 20$) at 1 mpt were analyzed by fluorescence-activated cell sorting (FACS) for expression of human CD45, CD19, and CD45, and mouse CD45 markers. Representatives (left) and the percentage of indicated markers (right) are shown. All cell populations were gated on mononuclear bone marrow cells. (B) Time course of human leukocyte development in the peripheral blood of IBMI-huNOG mice. Peripheral blood mononuclear cell (PBMC) from IBMI-huNOG mice ($n = 40$ for each time point) were stained for human CD45 at each time point. Box plots represent medians \pm 1.5 IQR. (C) Increased number of human lymphocytes in IBMI-huNOG mice. Absolute numbers of human CD45⁺ and CD3⁺ cells in peripheral blood were determined by FACS analysis at each time point ($n = 40$ for each time point). (D) CD4-CD8 ratio in peripheral blood T cells. The CD4-CD8 ratio was calculated as follows: [(CD4 T-cell numbers per μ L)/(CD8 T-cell numbers per μ L)] ($n = 40$). (E) Sustained composition of human leukocytes in peripheral blood. PBMCs from IBMI-huNOG mice ($n = 8$) were stained for human CD45, CD3, and CD19. Results are presented as mean percentages of human CD45⁺ cells.

HTLV-1 (Fuji Rebio).²³ To deplete human immunoglobulin M (IgM) or immunoglobulin G (IgG), streptavidin M-PVA magnetic beads (Chemagen) preincubated with biotin-conjugated goat anti-human IgM or IgG antibody (Sigma-Aldrich) were added to plasma from infected mice; a goat anti-mouse IgG antibody (Organon Teknika) was used as the negative control.

Bio-Plex cytokine assay

Plasma levels of IL-1b, IL-2, IL-4, IL-5, IL-6, IL-7, IL-8, IL-10, IL-12 (p70), IL-13, IL-17, granulocyte colony-stimulating factor (G-CSF), granulocyte macrophage colony-stimulating factor (GM-CSF), interferon- γ (IFN- γ), MCP-1, MIP-1 β , and tumor necrosis factor α (TNF- α) in HTLV-1-infected and control mice were analyzed using the Bio-Plex Human Cytokine 17-Plex Panel (Bio-Rad) on a Bio-Plex 200 system according to the manufacturer's instructions.

Statistical analysis

The significance of differences was determined by Mann-Whitney U test, paired t test, or Spearman's rank-correlation coefficient (r); $P < .05$ was considered to indicate statistical significance.

Results

Reconstitution of human immune cells in NOG mice using IBMI

IBMI-huNOG mice were generated by IBMI of human CD133⁺ hematopoietic stem cells into sublethally irradiated 6- to 7-week-old NOG mice. After 1 month of transplantation, human CD45⁺ leukocytes were found to have almost completely reconstituted the bone marrow of recipient mice (Figure 1A). At this time point, the majority of the human leukocytes in bone marrow consisted of CD19⁺ cells. A substantial number of CD34⁺ cells were also detected, whereas human CD3⁺ cells had not developed.

Less than half of peripheral blood cells were composed of human leukocytes even at 2 months posttransplantation (mpt).

However, the number of human leukocytes increased in a time-dependent manner (Figure 1B-C). Between 3 and 4 mpt, the number of human CD3⁺ T cells in the peripheral blood increased dramatically, as did the CD4-CD8 ratio (Figure 1D). CD3⁺ T cells and the CD4-CD8 ratio reached stable levels by 4 to 5 mpt, suggesting that the development of human T cells was completed within this period.

Previous reports have shown that reconstituted human CD45⁺ cells in other types of humanized mouse systems were overcome by CD3⁺ T cells within several months of transplantation due to the reduction of B-cell development,^{21,34} which may impair the integrity of host immunity. In contrast, the IBMI-huNOG mice model maintained a stable number of CD3⁺ T cells as well as the B- to T-cell ratio in peripheral blood through at least 8 mpt (Figure 1E). Thus, the human immune system appeared to be effectively reconstituted in IBMI-huNOG mice, likely due to the enriched repopulation of long-term hematopoietic stem cells by direct injection of CD133⁺ cells into the bone marrow cavity.²⁷

Proliferation of HTLV-1-infected T cells in IBMI-huNOG mice

Human T lymphocytes fully developed in IBMI-huNOG mice within 4 to 5 mpt. These mice were then infected with HTLV-1 by intraperitoneal inoculation with 2.5×10^6 irradiated MT2 cells. The number of human CD45⁺ leukocytes began to increase as early as 4 to 6 weeks postinoculation (wpi) and continued to increase rapidly thereafter (Figure 2A). HTLV-1 infection was also detected by 2 wpi, with the HTLV-1 PVL in peripheral blood increasing in a time-dependent manner (Figure 2B). The proportion of CD3⁺/CD45⁺ T lymphocytes was significantly enriched in HTLV-1-infected mice relative to mock-infected controls (Figure 2C), consistent with previous results.¹⁶ Absence of residual MT2 cells used as the source of HTLV-1 was confirmed by MT2 cell-specific PCR as previously described (supplemental Figure 1).³⁵

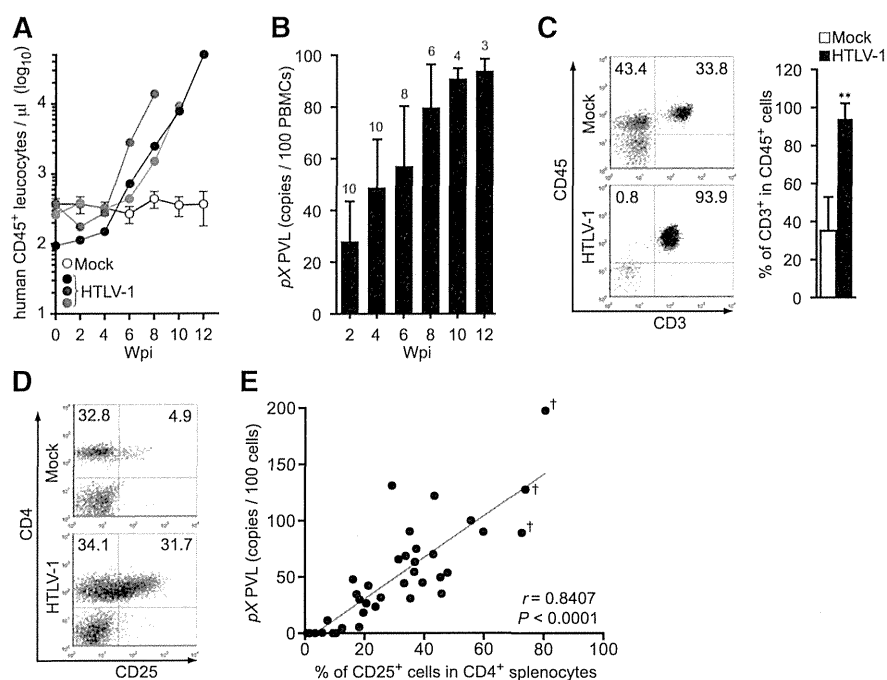


Figure 2. Kinetic analysis of HTLV-1 provirus in infected IBMI-huNOG mice. (A) Quantification of leukocyte numbers in the peripheral blood of HTLV-1-infected mice. Peripheral blood was routinely collected from mock- and HTLV-1-infected mice every 2 weeks. Human CD45⁺ leukocytes were enumerated by FACS. Results from mock-infected mice ($n = 10$) are presented as mean \pm standard deviation (SD), and representative results of 3 HTLV-1-infected mice are shown. (B) Quantification of HTLV-1 PVL in the peripheral blood of HTLV-1-infected mice. The PVL was determined by real-time PCR. Number at the top of each bar represents the number of analyzed HTLV-1-infected mice at each time point. (C) Expansion of CD3⁺ T-cell populations in the peripheral blood of HTLV-1-infected mice. PBMCs from mock-infected ($n = 3$) and HTLV-1-infected mice ($n = 18$) were stained for human CD3 when sacrificed; the median value was 8 wpi. Results are presented as the average percentages \pm SD of human CD45⁺ cells. (D) Expansion of CD25⁺ CD4 T cells in the spleen of HTLV-1-infected mice. Splenocytes were stained for human CD3, CD4, and CD25 and analyzed by FACS. Representative results from mock-infected (mouse ID: 8X20) and HTLV-1-infected (mouse ID: 8X01) mice are shown. (E) Correlation between the percentages of CD25⁺ T cells and PVLs in the spleen. HTLV-1-infected mice ($n = 37$) were sacrificed to determine PVL and CD25⁺ T-cell frequency in CD4⁺ splenocytes. One dot represents the result of an individual HTLV-1-infected mouse. Spearman's rank-correlation coefficient (r) was adopted to identify statistically significant correlations between values. Daggers indicate that flower cells were observed in the peripheral blood of HTLV-1-infected mice.

HTLV-1-infected humanized mice showed marked expansion of CD25⁺ CD4 T cells in the spleen relative to mock-infected controls (Figure 2D; Table 1), as is observed in peripheral blood of ATL and HAM/TSP patients.^{9,36} Furthermore, PVLs in the spleen were significantly correlated with the rate of CD25⁺ CD4 T cells (Figure 2E). These data suggest that the expanded CD25⁺ CD4 T-cell population represents the majority of HTLV-1-infected cells *in vivo*.

ATL-like leukemic symptoms in HTLV-1-infected IBMI-huNOG mice

The majority of HTLV-1-infected mice exhibited splenomegaly, while apparent infiltration of infected T cells in the liver was observed in 3 infected mice with flower cells (Figure 3A; Table 1) and the weight of liver in these mice was remarkably increased (HTLV-1: 1550 ± 620 mg [$n = 3$]; mock: 715 ± 85 mg [$n = 3$]). When PVLs of several lymphoid organs were analyzed, the proportions of infected cells in the bone marrow and lymph nodes were significantly lower than those in the spleen and peripheral blood, consistent with the leukemic phenotype of infected mice (Figure 3B). This result is in striking contrast to other humanized mouse models, in which HTLV-1 infection¹⁷ or the ectopic expression of Tax¹⁶ preferentially induce lymphoma.

May-Grunwald Giemsa staining of peripheral blood smears from infected mice revealed the presence of large, abnormal leukemic cells with lobulated nuclei, which were morphologically

identical to the flower cells observed in ATL patients (Figure 3D-E).⁸ The activated phenotype of infected T cells was also evident, with clear downregulation of CD3 expression on the surface of peripheral T cells in HTLV-1-infected mice, similar to that seen in ATL cells (Figure 3C).³⁷

ATL cells have been shown to secrete proinflammatory cytokines, such as IL-6, TNF- α , and GM-CSF, which stimulate activation and proliferation of infected T cells and promote development of ATL leukemogenesis.³⁸⁻⁴⁰ Analysis of cytokine and chemokine levels in the plasma of HTLV-1-infected mice revealed significantly elevated levels of several proinflammatory cytokines (Figure 4). The concentration of IFN γ significantly correlated with PVL in the peripheral blood (supplemental Figure 2), suggesting Th1 immune responses induced in infected mice. Together, these results suggest that HTLV-1-infected IBMI-huNOG mice accurately recreate many of the pathological features of ATL, including hepatosplenomegaly, leukemic T-cell overgrowth with lobulated nuclei, hypercytokinemia, and downregulation of CD3 on T cells.

Oligoclonal proliferation of human T-cell clones in HTLV-1-infected IBMI-huNOG mice

To evaluate the clonal proliferation of HTLV-1-infected T cells in infected mice, we quantified cellular clonality using clone-specific real-time PCR analysis. Splenocytes were isolated from 8 infected mice sacrificed at various time points, and genomic DNA fragments

Table 1. Pathological features of mock- or HTLV-1-infected IBMI-huNOG mice

Mouse ID*	Wpi†	PVL‡	CD3 ⁺ CD4 ⁺ (%)§	CD4 ⁺ CD25 ⁺ (%)§	Spleen weight (mg)	Lymph node weight (mg)	Observations
8807	—	—	16.7	2.6	45	1	Mock infected
8X10	—	—	20.2	3.4	51	3	Mock infected
8X20	—	—	36.5	4.4	40	2	Mock infected
8401	17	65.6	53.1	31.4	195	23	
8402	11	0.1	5.3	0.7	26	1	
8403	14	0.1	10.8	3.4	35	1	
8404	17	5.4	53.4	18.3	68	2	
8405	12	11.3	30.3	7.6	59	14	
8406	5	0.1	10.5	1.5	33	3	
8407	8	4.5	69.6	12.5	166	9	
8801	25	0.1	59.6	10.4	187	7	
8803	30	0.4	38.6	5.8	55	11	
8804	23	0.1	46.6	9.5	105	5	
8805	8	70.0	57.0	43.1	233	37	Leukemia
8808	8	26.5	52.5	20.6	101	40	
8810	4	42.2	55.4	21.3	40	22	
8X01	5	44.9	65.8	39.5	208	11	
8X04	8	121.9	62.2	43.5	165	7	Leukemia
8X05	23	127.7	81.4	73.9	226	8	Leukemia, flower cells (10.6%),¶ tumor lesion
8X06	9	31.6	50.5	25.5	155	5	
8X09	5	34.6	52.2	17.4	227	9	
8X12	4	47.9	58.5	16.2	188	11	
8X14	25	68.6	51.4	33.8	145	25	Leukemia
8X16	7	90.4	78.9	35.2	200	16	Leukemia
8X17#	9	131.1	44.6	29.3	200	35	Leukemia
8X18	18	197.7	89.4	80.5	358	28	Leukemia, flower cells (19.2%),¶ tumor lesion
9Z01	10	53.6	75.8	47.9	220	12	Leukemia
9Z03	6	23.4	51.6	23.7	38	18	
9Z17	6	18.2	64.7	19.7	163	10	
9Z18	16	89.2	80.4	72.7	285	5	Leukemia, flower cells (4.2%),¶ tumor lesion
9Z19	6	35.0	65.0	45.9	207	20	
X202	12	90.0	76.6	59.9	353	13	Leukemia
X206	8	54.4	56.6	36.7	317	15	
X207**	11	100.0	62.2	55.7	358	6	Leukemia
X208	4	29.9	74.7	18.4	188	15	
X209	7	30.8	74.4	35.4	270	21	
X212	9	74.9	56.8	37.4	270	5	Leukemia
X214	10	44.3	48.0	33.3	170	6	
X216	8	63.2	66.1	36.9	271	12	Leukemia
X217	7	49.6	76.9	45.5	306	18	Leukemia

Leukemia, infected mice with atypical lymphocytes >90% of PBMCs; flower cells, atypical lymphocytes with >4 lobulated nuclei in a cell; tumor lesion, tumor formation of infiltrating infected T cells in the liver.

*The 37 infected mice listed are identical to those in Figure 2E.

†The wpi when indicated mice were sacrificed.

‡PVL is expressed as number of *pX* copies per 100 cells.

§The population of indicated marker-positive cells in CD45⁺ splenocytes.

||The weight value of one of the largest mesenteric lymph node in each mouse.

¶The percentage of flower cells in total lymphocytes in blood smear (presented in parentheses).

#High proportion of CD25⁺ CD8 T cells in PBMCs.

**High proportion of DP T cells in PBMCs.

flanking the major integration sites in the HTLV-1-infected cells were amplified by IL-PCR. Amplified DNA fragments were subcloned into plasmids and sequenced to confirm proper integration (supplemental Table 5). As shown in Figure 5A, the occupancy of detected clones determined by real-time PCR was < 5% in cells harvested 5 to 8 wpi, indicating polyclonal HTLV-1 infection in these mice. In contrast, 2 mice sacrificed after prolonged infection periods (18 and 23 wpi, respectively) produced high percentages of infected clones. Interestingly, these 2 mice also showed overgrowth of CD25⁺ CD4 T cells with flower-shaped nuclei, characteristic of ATL cells (Figure 3D-E), whereas such cells were not observed in the 6 remaining mice. These findings indicate that a limited number of HTLV-1-infected T-cell clones

selectively proliferated in the spleens of infected mice, resulting in an ATL-like leukemic phenotype.^{33,41}

Presence of identical infected clones in CD25⁻ and CD25⁺ CD4 T-cell populations

Splenocytes from infected mice were sorted into CD25⁻ or CD25⁺ CD4 T cells and CD8 T cells; the PVL of each population was also determined. Most of the CD25⁺ CD4 T cells isolated from the spleens of infected mice were provirus-positive, as was a significant proportion of CD25⁻ CD4 T cells, whereas infection of CD8 T cells was rare (Figure 5B). Interestingly, *tax* expression in HTLV-1-infected CD25⁺ CD4 T cells was suppressed compared with that in

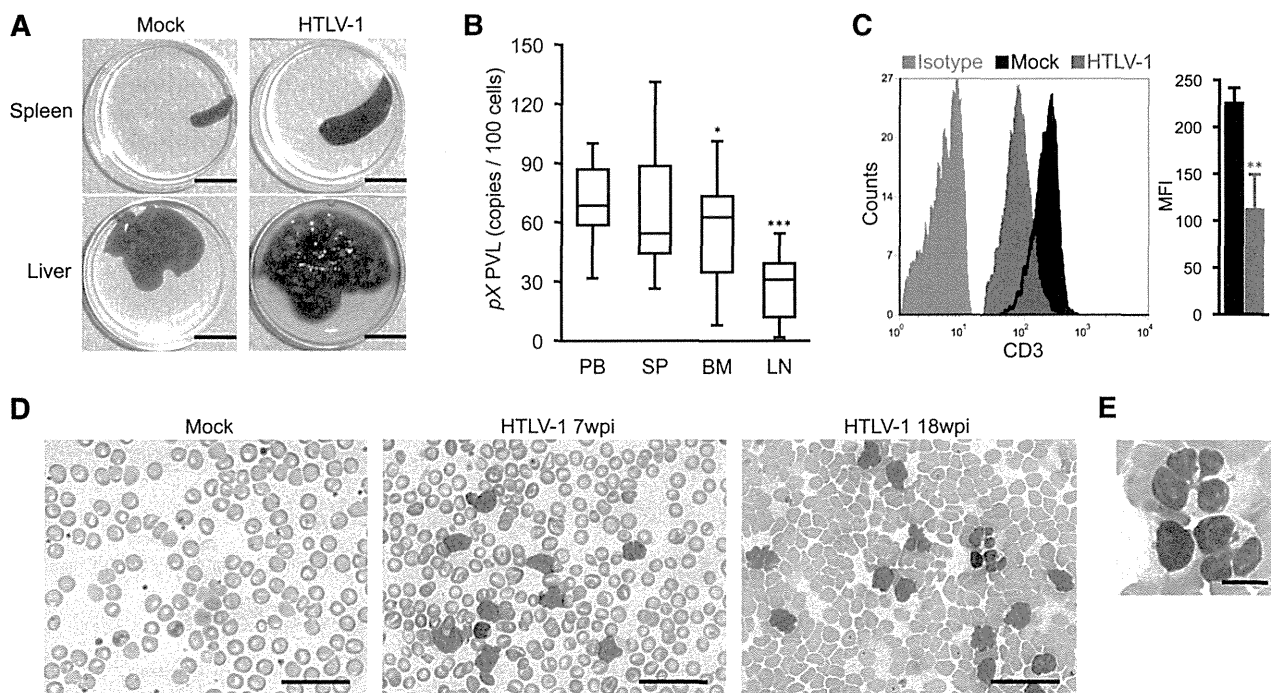


Figure 3. Splenomegaly and leukemic T-cell overgrowth in infected IBMI-huNOG mice. (A) Hepatosplenomegaly in HTLV-1-infected mice. Representative spleens and livers from mock- and HTLV-1-infected mice are shown. Scale bars in panel A represent 10 mm. (B) PVL in lymphoid organs of HTLV-1-infected mice. PVL in the peripheral blood (PB), spleen (SP), bone marrow (BM), and lymph nodes (LN) of HTLV-1-infected mice ($n = 17$) are shown. Box plots represent medians ± 1.5 IQR. Asterisks indicate statistical significance vs the value obtained from peripheral blood (* $P < .05$, *** $P < .001$ by paired t test). (C) Downregulation of CD3 on the T-cell surface. PBMCs from mock- ($n = 3$) and HTLV-1-infected mice ($n = 18$) were stained for human CD3 and analyzed by FACS. Results are presented as mean MFI \pm SD of CD3 expression. (D-E) Smears of peripheral blood from HTLV-1-infected mice showing a number of leukemic cells with atypically shaped nuclei. Results from two infected mice (7 and 18 wpi, respectively) and a mock-infected mouse (at 8 wpi) are shown. Higher-magnification view of flower cells in panel D is shown in panel E. Scale bars in panels D-E represent 50 and 10 μ m, respectively. Asterisks in panels B and C represent significant differences vs mock-infected mice (** $P < .01$ by Mann-Whitney U test).

CD25⁻ CD4⁺ T cells; however, higher *HBZ* expression was observed in CD25⁺ CD4⁺ T cells (Figure 5C).

Further clonality analysis for HTLV-1-infected CD25⁻ and CD25⁺ CD4⁺ T cells isolated from the same spleen with the purity of >95% (supplemental Figure 3) revealed that the most abundant clone was the same in both T-cell populations; however, the occupancy was higher in the CD25⁺ population (Figure 5D), indicating the preferential growth of infected clones with CD25 expression.

Induction of HTLV-1-specific adaptive immune responses in HTLV-1-infected IBMI-huNOG mice

HLA-A*24:02-restricted Tax-specific CTLs were frequently detected in ATL patients, and are known to play an important role in the control of HTLV-1-infected cells in vivo.⁴²⁻⁴⁴ To investigate whether Tax-specific CTLs were induced in HTLV-1-infected mice, the IBMI-huNOG mice were generated using hematopoietic stem cells purified from the cord blood of an HLA-A*24:02 haplotype individual. HLA-A*24:02 tetramers coupled with Tax301-309 were used to detect CTLs. The cord blood HLA-A alleles used in this study are shown in supplemental Table 1. As shown in Figure 6A, Tax301-309-specific CTLs were detected in HTLV-1-infected mice at a frequency similar to that of ATL patients (0.7% \pm 0.8%, $n = 18$),⁴⁵ whereas control tetramer CTLs specific for HIV env produced only marginal staining of CD8 T cells.

To evaluate whether functionally reactive Tax301-309-specific CTLs were present in infected mice, we cultured splenocytes from HTLV-1-infected mice in the presence of Tax peptide. Tax301-309 specific CTLs clearly proliferated following peptide stimulation; no reaction was seen in controls. Furthermore, the frequency

of Tax301-309-specific CTLs in in vivo CD8 T cells was inversely correlated with the PVLs of HTLV-1-infected mice (Figure 6B). These results suggest that HTLV-1-infected mice induce functional T-cell-mediated cellular immunity against HTLV-1, which may be involved in the control of HTLV-1-infected cells in vivo.

Antibodies against HTLV-1 antigens were also detected in the plasma of infected mice as early as 2 wpi, whereas the specific antibody was not detected before infection (Figure 6C). The titer of HTLV-1-specific antibodies increased in all cases until 4 wpi, followed by a gradual decline in 67% of infected mice (4 of 6), coincident with a decrease in body weight. However, 2 of the infected mice exhibited a reactivation of antibody production at 8 wpi, suggestive of immunoglobulin class switching from IgM to IgG. In fact, HTLV-1-specific antibody titers were significantly decreased following selective depletion of human IgG, indicating the presence of functional IgG in the plasma of HTLV-1-infected mice (Figure 6D). These data clearly support the notion that the functional interaction between human T and B cells required for class switching exists in this model. Taken together, these results demonstrate that human-like adaptive immunity against HTLV-1 was established in the HTLV-1-infected IBMI-huNOG mice.

Discussion

In this study, we established a novel humanized mouse model of HTLV-1 infection. To generate humanized mice, we transplanted